Astron. Astrophys. 353, 528–542 (2000)

ASTRONOMY AND ASTROPHYSICS

Elemental abundances of carbon, nitrogen, and oxygen in carbon stars⋆

K. Ohnaka[1,2,⋆⋆], **T. Tsuji**[1], **and W. Aoki**[3]

[1] Institute of Astronomy, University of Tokyo, 2-21-1 Osawa, Mitaka, Tokyo, 181-8588 Japan
[2] Technische Universität Berlin, Institut für Astronomie und Astrophysik, Hardenbergstrasse 36, 10623 Berlin, Germany
[3] National Astronomical Observatory of Japan, 2-21-1 Osawa, Mitaka, Tokyo, 181-8588 Japan

Received 21 September 1999 / Accepted 8 November 1999

Abstract. The elemental abundances of carbon, nitrogen, and oxygen in three carbon stars (TX Psc, V Aql, and BL Ori) are determined from high-resolution infrared spectra in a self-consistent manner, with the dependence of the atmospheric structure on the chemical composition fully taken into account. For this purpose, we have constructed a grid of line-blanketed model atmospheres using a revised Band Model opacity.

The derived carbon, nitrogen, and oxygen abundances show good agreement with the result obtained by Lambert et al. (1986) in most cases. The differences between the two groups are typically within 0.1 dex, which is remarkable for abundance analyses, especially for very cool stars. Since our model atmospheres and the method of the analysis are independent of their work, this result lends a support to the consistency of the analyses by the both groups.

However, accurate determination of C/O ratio has turned out to be extremely difficult. The C/O ratios which are derived even with the same stellar parameters with those adopted by Lambert et al. (1986) are somewhat larger than their results: 1.07 (TX Psc), 1.47 (V Aql), and 1.07 (BL Ori), while their results are 1.027 (TX Psc), 1.25 (V Aql), and 1.039 (BL Ori). Moreover, the resulting abundances are rather sensitive to the effective temperature and the surface gravity. It is possible that the effective temperature scale is higher by 100 – 200 K than that Lambert et al. (1986) adopted, and in that case, C/O ratios in three stars become still systematically higher than those derived by Lambert et al. (1986), showing a contrast to their conclusion that the majority of carbon stars have C/O ratios rather close to 1. In fact, the C/O ratios derived here are 1.17 (TX Psc), 1.74 (V Aql), and 1.19 (BL Ori). A decrease of the surface gravity from $\log g$ = 0.0 to -0.5 also leads to an increase of C/O ratio by 10%. In other words, given the uncertainties of stellar parameters and molecular data in addition to internal errors, it is still difficult to determine C/O ratios within accuracy of 10%, which can be translated to a difference between C/O = 1.02 and 1.1.

The $^{12}\mathrm{C}/^{13}\mathrm{C}$ ratios in N-type carbon stars derived in our previous analysis have been revised with the new model grid. The $^{12}\mathrm{C}/^{13}\mathrm{C}$ ratios in three stars have turned out to be 31 (TX Psc), 74 (V Aql), and 35 (BL Ori), larger by about 40% than those we obtained previously. And the C/O ratios and the $^{12}\mathrm{C}/^{13}\mathrm{C}$ ratios derived here fall within the range predicted by the addition of ^{12}C to the atmosphere of K and M giants. It supports the scenario in which K and M giants evolve to carbon stars as ^{12}C synthesized in the thermal pulse is dredged-up.

Key words: stars: abundances – stars: atmospheres – stars: carbon – stars: AGB and post-AGB

1. Introduction

Intermediate- and low-mass stars ($1M_{\odot} < M < 8M_{\odot}$) undergo the modification of the photospheric chemical composition at the asymptotic giant branch (AGB), as material synthesized via nuclear processes is dredged up into the stellar surface. The nuclear burning in AGB stars is characterized by the double shell burning: the unstable helium burning, so-called thermal pulse, taking place at the bottom of the helium shell, and the hydrogen burning at the bottom of the hydrogen envelope. The dredge-up of ^{12}C freshly synthesized via the 3α process in the thermal pulse leads to the drastic change of the surface chemical composition from oxygen-rich to carbon-rich. However, theoretical calculations of the evolution of AGB stars still fail to reproduce observational facts like the luminosity functions of carbon stars in the Magellanic Clouds. On the other hand, the chemical composition of carbon stars provides us with a unique opportunity to shed light on nucleosynthesis and mixing processes taking place in the stellar interior. Moreover, the determination of the surface chemical composition, especially C/O ratio, has a large impact on the understanding of the physics and the chemistry of the circumstellar envelope like dust formation and the mass loss mechanism.

Lambert et al. (1986, hereafter LGEH86) analyzed the elemental abundances of carbon, nitrogen, and oxygen, as well as

Send offprint requests to: K. Ohnaka (Present address below)

⋆ Table 1 is only available in electronic form at the CDS via anonymous ftp to cdsarc.u-strasbg.fr (130.79.128.5) or via http://cdsweb.u-strasbg.fr/Abstract.html

⋆⋆ *Present address:* Department of Astronomy, School of Science, University of Tokyo, 7-3-1 Hongo, Bunkyo-ku, Tokyo, 113-0033 Japan
Correspondence to: ohnaka@mtk.ioa.s.u-tokyo.ac.jp

$^{12}C/^{13}C$ ratios in 30 carbon stars from high-resolution infrared (1.5–2.5 μm) spectra. On the other hand, Ohnaka & Tsuji (1996, hereafter OT96) analyzed $^{12}C/^{13}C$ ratios in 62 N-type carbon stars from the CN red system lines around 8000 Å, and found a systematic discrepancy compared with the result derived by LGEH86 for 20 stars analyzed by the both authors. In order to investigate the reason for this disagreement and to examine the possible effects of model atmospheres on elemental abundance analyses, Ohnaka et al. (1998, hereafter OTAY98) re-analyzed the original spectra of 3 carbon stars (TX Psc, V Aql, and BL Ori) that LGEH86 acquired, and determined elemental C and O abundances using independent model atmospheres. The resulting oxygen abundances in the three stars showed good agreement with those obtained by LGEH86, while C/O ratios were found to be systematically larger than their results.

Recently we have carried out the revision of the molecular opacity used in the calculation of our model atmospheres. The effect of the molecular absorption due to CO, CN, C_2, HCN, and C_2H_2 is taken into account using the Band Model method, not on a line-by-line basis like the Opacity Sampling method. We have revised and verified the Band Model opacity by comparing emergent fluxes predicted with the Band Model with synthetic spectra calculated on a line-by-line basis. Besides, we have incorporated the opacities due to CH, CS, CaH, MgH, FeH, SiO, C_3, and CH_4 as well as due to 4 isotopic species, ^{13}CO, ^{13}CN, $^{12}C^{13}C$, and $^{13}C^{13}C$.

In the present work, we present the analysis of elemental C, N, and O abundances using model atmospheres computed with this revised molecular opacity. The atmospheric structure of carbon stars is quite sensitive to the chemical composition, especially C/O ratio, since, with most of oxygen atoms locked up into CO molecules, the amount of other carbon-bearing molecules is dependent on C/O ratio. The analysis is done using a grid of model atmospheres so that the sensitivity of the atmospheric structure to the chemical composition should properly be taken into account. We also discuss the effects of the uncertainties of stellar parameters on the resulting abundances. In Sect. 2 and Sect. 3, we describe the observational data and line identification, respectively. In Sect. 4 the revision of the Band Model opacity and its effect on the atmospheric structure are presented. Sect. 5 describes the method of the analysis of C, N, and O abundances. The result and the uncertainties are discussed in Sect. 6. In Sect. 7, we present the tests of model atmospheres based on spectrophotometric observations, and address the accuracy of abundance analyses concerning cool carbon stars and difficulties still remaining to be overcome. We also discuss the effect of the new models on the $^{12}C/^{13}C$ ratios we previously derived. At the end, the evolution of carbon stars is discussed in terms of C, N, and O abundances as well as $^{12}C/^{13}C$ ratios.

2. Observational data

The spectra analyzed in the present work were originally obtained by LGEH86, using the Mayall reflector at Kitt Peak National Observatory and the Fourier transform spectrometer (FTS). The spectra of all 32 stars observed were kindly made available to us by Dr. K. H. Hinkle. The region from 4000 to 6600 cm^{-1} (2.5–1.5 μm) is covered with a resolution of 0.0412 cm^{-1}. After apodizing the spectra by Norton & Beer (1976) apodizing function I2, the actual resolution is 0.0696 cm^{-1}. The S/N ratios after the apodization are 146 (TX Psc), 103 (V Aql), and 61 (BL Ori), demonstrating the high quality of the data.

Here we select 3 stars for a study of the effects of model atmospheres on the analysis of elemental abundances: TX Psc, V Aql, and BL Ori. These stars are primarily selected for their effective temperatures. Namely, the effective temperatures of these stars are 3080 K (TX Psc), 2790 K (V Aql), and 3180 K (BL Ori) (OT96). We will mention the effective temperature scale in Sect.4.2 again.

3. Line identification

One of the advantages of analyzing infrared spectra is the lower line density than in the optical region, which not only helps us define the continuum level well but also makes it easier to select isolated lines. The observed spectra show rich molecular absorption due to CO, C_2, and CN, which are used for the determination of oxygen, carbon, and nitrogen abundances, respectively. Though the line density in the infrared is not as high as in the optical region, it still poses difficulties in selecting isolated lines.

Since the region between 5100 and 5500 cm^{-1} is severely contaminated by telluric absorption, we determine the continuum level separately in the H-band (5500–6400 cm^{-1}) and in the K-band (4000–5100 cm^{-1}). The continuum level is defined by drawing an envelope over the peaks in each spectrum.

The line list of the CO first- and second-overtone bands is the same with that used for the analysis of CO lines in M-giants by Tsuji (1986, 1991). Our line list of CO includes $^{12}C^{16}O$, $^{13}C^{16}O$, $^{12}C^{17}O$, and $^{12}C^{18}O$. Fig. 1 shows a portion of spectra of TX Psc, V Aql, and BL Ori in the H-window, together with the positions of some ^{12}CO lines selected for the analysis.

We only use the CO second-overtone lines for the abundance analysis. The first-overtone lines, which are generally formed in the upper layers, are a good probe of the outer atmosphere and the inner circumstellar envelope, but not suitable for an abundance analysis. In fact, Tsuji (1991) reveals that the CO first- and second-overtone lines give different carbon abundances in the case of M giants. The first-overtone lines, especially low excitation lines, should be investigated for the understanding of the outer atmosphere, only after the photospheric model is fixed by an abundance analysis using weak lines.

The C_2 Phillips system originating from transitions $A\,^1\Pi$ – $X\,^1\Sigma^+$ can be used for an indicator of the carbon abundance. Because of the relative simplicity of the singlet sigma state, energy levels, therefore, line positions and lower excitation potentials can be calculated with accurate molecular constants. Douay et al. (1988) recorded an infrared spectrum of C_2 and analyzed 12 bands: $0-0, 3-3, 4-4, 5-5, 0-1, 1-2, 2-3, 0-2, 1-3, 2-4, 3-5$, and $4-6$. They derived molecular constants such as T_v, B_v, and H_v up to $v = 6$ for the $X\,^1\Sigma^+$ state and $v = 5$ for

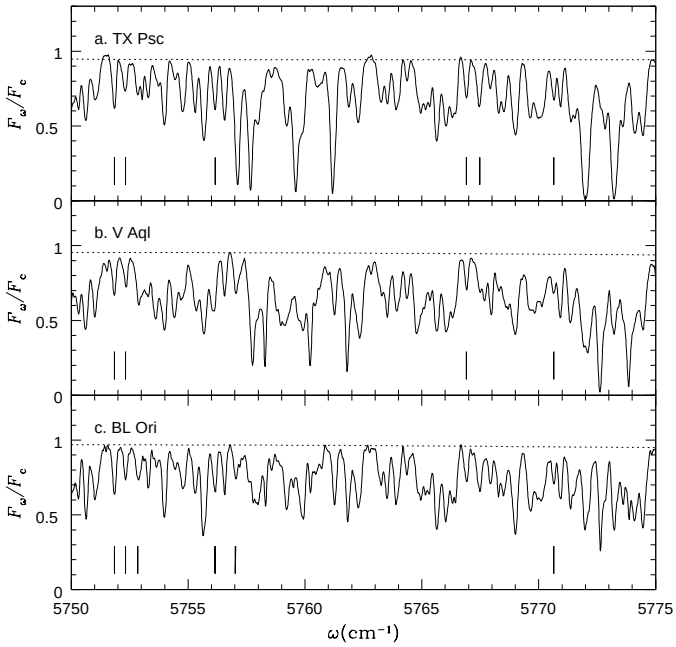

Fig. 1. A portion of spectra of TX Psc, V Aql, and BL Ori. The ticks indicate ^{12}CO lines selected for the analysis. The dotted lines represent the continuum levels

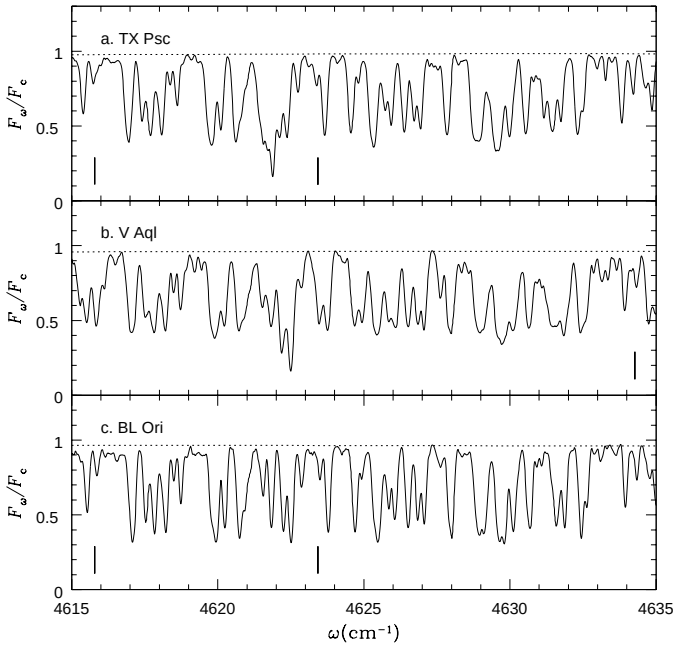

Fig. 2. A portion of spectra of TX Psc, V Aql, and BL Ori. The ticks indicate $^{12}C_2$ lines selected for the analysis. The dotted lines represent the continuum levels

the $A\,^1\Pi$ state. Our line list of the C_2 Phillips system is generated using their molecular constants. Fig. 2 illustrates a portion of the observed spectra, where C_2 lines are identified. Despite its crucial role in the determination of the carbon abundance, the number of C_2 lines finally selected for the analysis is quite limited mainly due to the blending of CN lines. We selected 5 lines for TX Psc, 8 lines for V Aql, and 7 lines for BL Ori, and those lines originate from (0,2) and (1,3) bands.

The gf-value of an individual line of the Phillips system is given by

$$gf = f_{v'v''}\frac{S_{J'J''}\omega}{2\omega_{v'v''}}, \quad (1)$$

where $f_{v'v''}$ is the band oscillator strength, $S_{J'J''}$ is the Hönl-London factor, ω is the wavenumber of the individual line, and $\omega_{v'v''}$ is the wavenumber of the band origin of (v', v'') band. It is here assumed that the electronic dipole moment is independent of the internuclear distance. The Hönl-London factors are $S_{J'J''} = 2J'' + 1$ for the Q-branch, $S_{J'J''} = J'' - 1$ for the P-branch, and $S_{J'J''} = J'' + 2$ for the R-branch. The oscillator strengths of the Phillips system are still of controversy. The experimental results obtained by Davis et al. (1984) and Bauer et al. (1985) show $f_{00} = 1.38 \times 10^{-3}$. However, the ab initio calculation performed by Langhoff et al. (1990) shows a remarkably larger value, $f_{00} = 2.28 \times 10^{-3}$. In addition, Grevesse et al. (1991) derived the oscillator strengths of the Phillips system from the solar spectrum, and their result is reported to be in agreement with the theoretical values derived by Langhoff et al. (1990). On the other hand, LGEH86 adopted a compromise of the values which were then available. Because one of our purposes lies in the investigation of the effects of model atmospheres in comparison with the analysis by LGEH86, we adopt the values used in their analysis. Namely, we adopt $f_{02} = 2.5 \times 10^{-4}$ and $f_{13} = 3.8 \times 10^{-4}$ for the band oscillator strengths of (0,2) and (1,3) bands, respectively.

Regarding CN molecule, Cerny et al. (1978) recorded an infrared spectrum of the red system ($A\,^2\Pi$ – $X\,^2\Sigma^+$) and analyzed 14 bands of $\Delta v = +1$, 0, -1, and -2 sequences. Line positions are computed with the formulae and the molecular constants given in their work. Line positions of ^{13}CN are also computed, using the molecular constants determined by Hosinsky et al. (1982). Fig. 3 shows some CN lines identified in the spectra of three stars.

Unfortunately the oscillator strengths of the red system are also controversial. The experiment done by Davis et al. (1986) resulted in a value of $f_{00} = 1.94 \times 10^{-3}$. On the other hand, the ab initio calculations performed by Larsson et al. (1983) and Bauschlicher et al. (1988) resulted in larger values. The result obtained by Larsson et al. (1983) is $f_{00} = 2.28 \times 10^{-3}$, while that derived by Bauschlicher et al. (1988) is $f_{00} = 2.361 \times 10^{-3}$. Those theoretical values also agree with the oscillator strengths derived from the analysis of the solar spectrum (Sneden & Lambert 1982). LGEH86 adopted the values of the ab initio calculation by Larsson et al. (1983). As we mentioned in the case of the C_2 Phillips system, we adopt the same values with those used by LGEH86.

The dissociation energy of CN ($D_0(\mathrm{CN})$) is also in dispute. Costes et al. (1990) discuss the results determined with various experimental and theoretical methods since 1973, and $D_0(\mathrm{CN})$ ranges from 7.18 to 8.05 eV. Since $D_0(\mathrm{CN})$ has a direct effect on the determination of nitrogen abundances, we adopt the value employed by LGEH86, 7.60 eV.

The lines selected for the analysis are listed in Table 1.

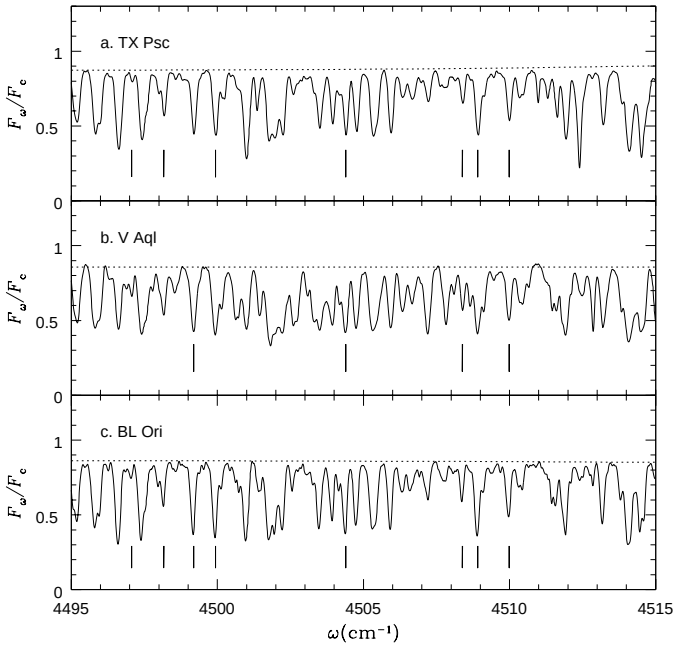

Fig. 3. A portion of spectra of TX Psc, V Aql, and BL Ori. The ticks indicate ^{12}CN lines selected for the analysis. The dotted lines represent the continuum levels

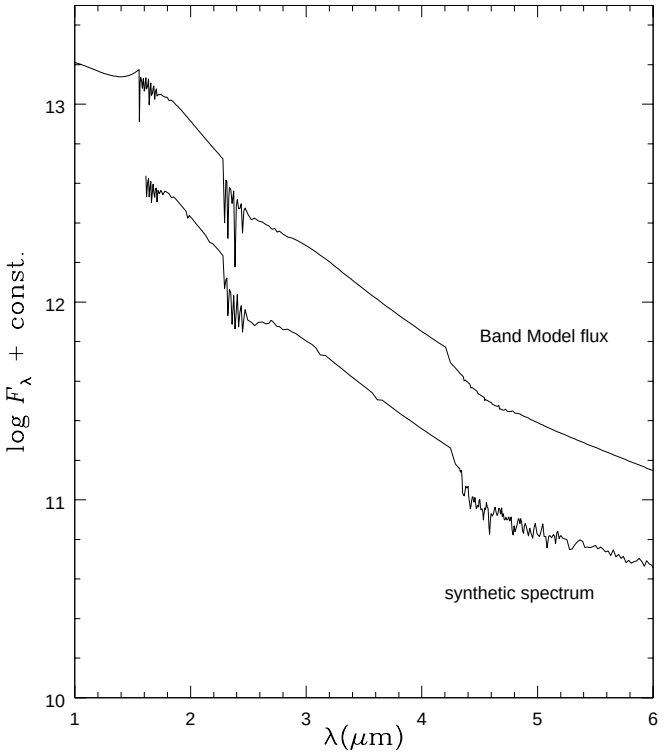

Fig. 4. Comparison between a Band Model flux and a synthetic spectrum of CO absorption. The model used in both calculations has $T_{\rm eff}$ = 3000 K, $\log g$ = 0.0, C/O = 1.1, [O/H] = [N/H] = 0.0, and $V_{\rm mic}$ = 3.0 km s^{-1}. The two spectra are offset in the vertical coordinate for clarity of presentation

4. Model atmospheres

4.1. Band model opacity

Our model atmospheres are based on four assumptions: hydrostatic equilibrium, plane-parallel geometry, local thermodynamical equilibrium (LTE), and radiative equilibrium. The effect of molecular line absorption is taken into account using the Band Model method (Tsuji 1994 and references therein). The Band Model method characterizes a run of opacity in a given spectral mesh by two parameters, namely, the mean absorption coefficient and the mean line separation. In other words, the frequency dependence of molecular line opacity in a spectral mesh is approximated with an array of lines with an equal intensity spaced at an equal interval. Once the mean absorption coefficient and the mean line separation are evaluated directly from the relevant molecular constants (see formulae in Tsuji 1994), it is straightforward to compute the opacity distribution function (ODF). This method has an advantage that the detailed calculation of the real frequency dependence of molecular line absorption is not necessary for the computation of the ODF. However, while the mean absorption coefficient can easily be calculated, we should be careful in evaluating the mean line separation. In a spectral mesh where many weak lines are present, the mean line separation might be unrealistically small, if all these weak lines are taken into account. Besides, another problem arises in the case of electronic transition bands like the CN red system, where weak lines due to the satellite branches are present. It is somewhat subtle whether these satellite branches should be considered in the evaluation of the mean line separation.

The best way to verify the evaluation of the mean line separation is to compare emergent fluxes calculated with the Band Model with synthetic spectra computed on a line-by-line basis. Using the temperature and pressure stratifications of some model, the absorption spectrum of a particular molecule can be calculated with the Band Model method. On the other hand, a synthetic spectrum is calculated using the same model and a detailed line list.

Fig. 4 shows a comparison between a Band Model flux and a synthetic spectrum of CO. Both the Band Model flux and the synthetic spectrum are calculated using a model with $T_{\rm eff}$ = 3000 K, $\log g$ = 0.0, C/O = 1.1, [O/H] = [N/H] = 0.0, and $V_{\rm mic}$ = 3.0 km s^{-1}. The figure shows that the synthetic spectrum is well reproduced by the Band Model flux, confirming the validity of the Band Model opacity in the case of CO vibration-rotation transitions.

We compare Band Model fluxes and a synthetic spectrum of the CN red system in Fig. 5. The model used in the calculations is the same as that used in the case of CO above. The mean line separation is evaluated in two manners: with the satellite branches taken into account or not. The number of main branches is 6 ($P_1, P_2, Q_1, Q_2, R_1, R_2$), while the number of the satellite branches is also 6 ($^O P_{12}, ^Q P_{21}, ^P Q_{12}, ^R Q_{21}, ^Q R_{12}, ^S R_{21}$). It means that the mean line separation evaluated with the satellite branches included is by a factor of 2 smaller than otherwise. In fact, the emergent flux calculated with the smaller line separation (Fig. 5a, dotted line) exhibits the deeper absorption compared with that calculated with the satellite branches neglected

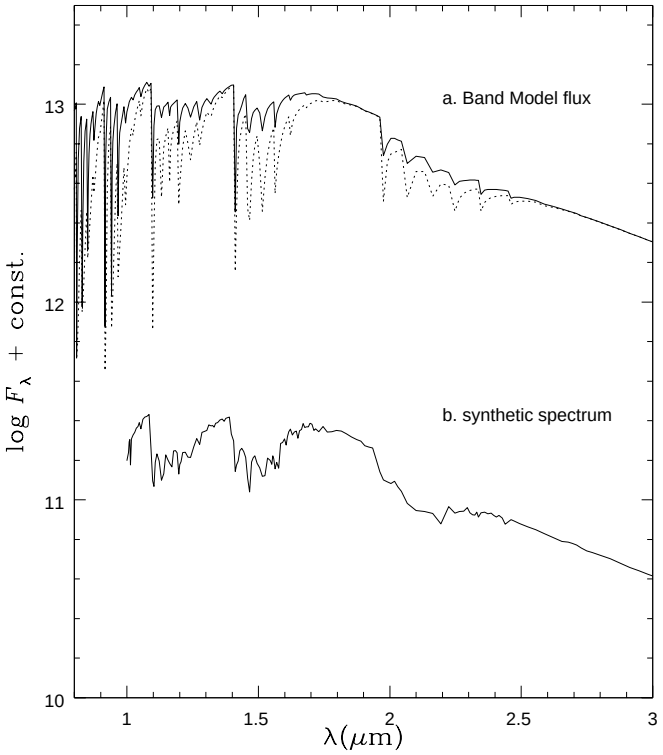

Fig. 5. The same with Fig. 4, but for the CN red system. **a.** The solid line represents an emergent flux calculated with the satellite branches neglected. The dotted line is the Band Model flux calculated with the satellite branches included. **b.** Synthetic spectrum. See also the text

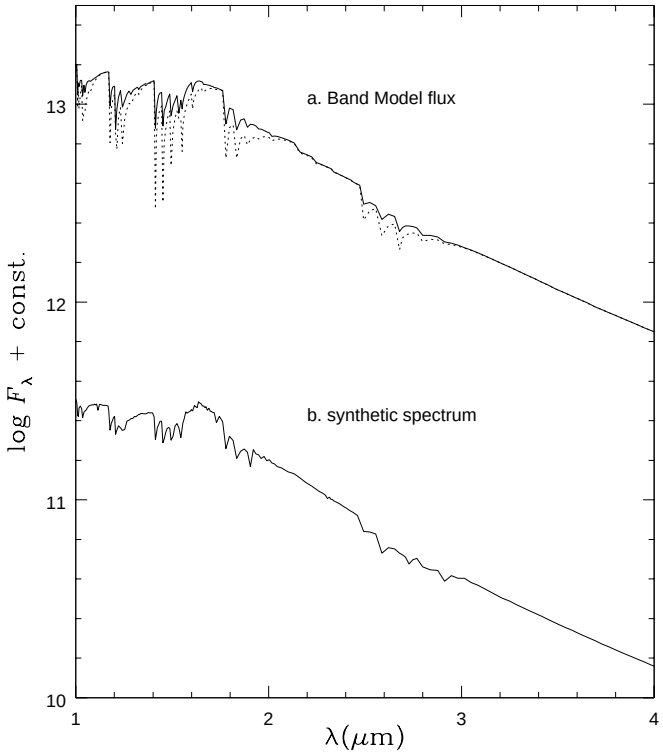

Fig. 6. The same with Fig. 4, but for the C_2 Ballik-Ramsey system. **a.** The solid line represents an emergent flux calculated with the revised Band Model opacity, reflecting the missing levels. The dotted line is the Band Model flux calculated with the narrower mean line separation. **b.** Synthetic spectrum. See also the text

(solid line). In our preceding analyses (OT96 and OTAY98), the satellite branches were taken into account in the evaluation of the mean line separation. Fig. 5 demonstrates that the synthetic spectrum lies between the two cases, but is better reproduced by the Band Model opacity with the satellite branches neglected.

Fig. 6 shows the same test for C_2 molecule. In the case of C_2 molecule, the mean line separation can be affected by *missing levels* which result from the fact that C_2 is a homonuclear molecule with a zero nuclear spin. Namely, lines with odd J fall out in the Phillips system, while in the Ballik-Ramsey system, lines with odd N fall out in the P- and R-branches and those with even N fall out in the Q-branch. Both cases suggest the reduction of the number of lines by a factor of 2 in a given spectral mesh, leading to an increase in the mean line separation by a factor of 2. In our preceding analyses, these missing levels were also included in the evaluation of the mean line separation. As Fig. 6 shows, however, the synthetic spectrum is better reproduced if the line separation is doubled, reflecting the missing levels.

We extend the list of molecules included in the model calculation beyond the 5 major opacity sources (CO, CN, C_2, HCN, C_2H_2). In the present work, we also include the opacities due to CH, CS, CaH, MgH, FeH, SiO, C_3, and CH_4 as well as due to 4 isotopic species, ^{13}CO, ^{13}CN, ^{12}C^{13}C, and ^{13}C^{13}C.

The effect of the revision of the opacity on the resulting temperature stratification is shown in Fig. 7 for a model with $T_{\rm eff}$ = 3000 K, $\log g$ = 0.0, C/O = 1.1, [O/H] = [N/H] = 0.0, ^{12}C/^{13}C = 25, and $V_{\rm mic}$ = 3.0 km s^{-1}. The larger line separations of CN and C_2 discussed above lead to a decrease in temperature by 100–200 K in the deeper layers and by $\sim$ 300 K in the upper layers, overwhelming the backwarming effect expected from the isotopic species or molecules like CaH, MgH, and FeH which have absorption features in the optical region. Fig. 8 shows a comparison of models with $T_{\rm eff}$ = 3200 K. The effect of the revision of the opacity is smaller in this case. In fact, the difference of the temperature stratifications is mostly 100–200 K. Therefore, the effect of the revision of the Band Model opacity is dependent on the effective temperature. The cooling resulting from the larger line separations promotes the formation of polyatomic molecules, which also work to cool down the atmosphere. In the case of $T_{\rm eff}$ = 3000 K models, the cooling effect due to the larger line separations is large enough to promote the formation of polyatomics in the upper layers. On the other hand, in the case of $T_{\rm eff}$ = 3200 K models, the formation of polyatomics is not so much promoted, resulting in the smaller difference of the temperature stratifications.

4.2. Stellar parameters and model grid

With the Band Model opacity thus revised, we compute a grid of model atmospheres. Our model atmospheres are specified

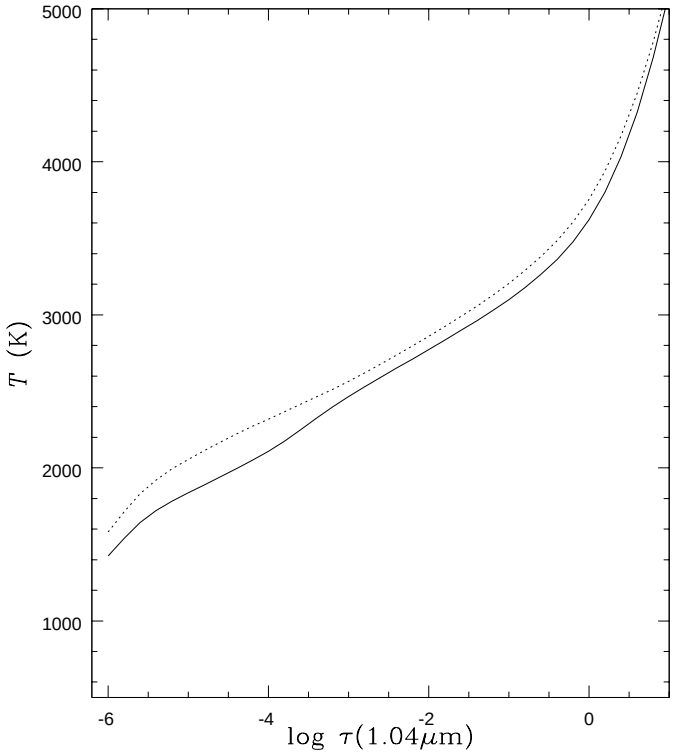

Fig. 7. Comparison of model atmospheres used in our preceding analyses and the present work. The solid line represents a model computed with the revised Band Model opacity, while the dotted line represents a model used in our previous analyses. The model parameters are $T_{\rm eff}$ = 3000 K, log g = 0.0, C/O = 1.1, [O/H] = [N/H] = 0.0, ^{12}C/^{13}C = 25, and $V_{\rm mic}$ = 3.0 km s^{-1}

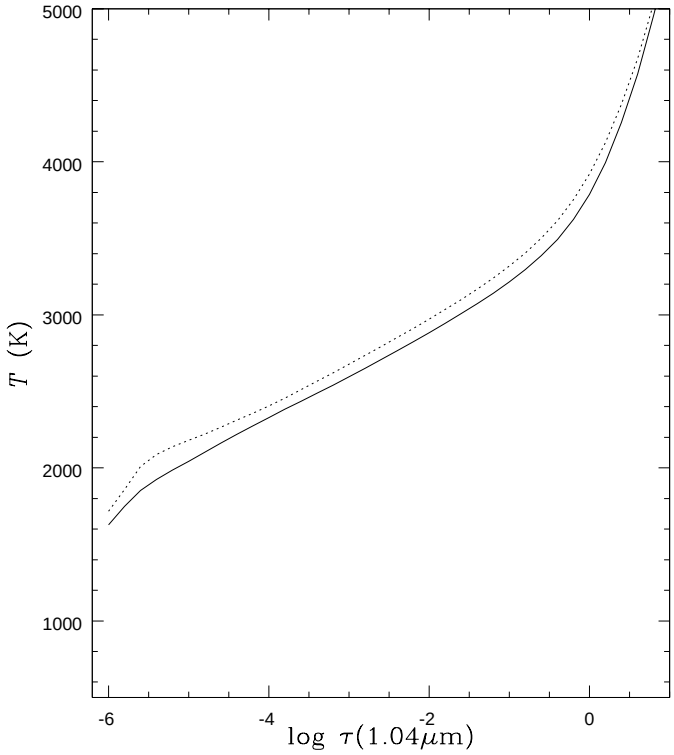

Fig. 8. Comparison of model atmospheres used in our preceding analyses and the present work. The solid line represents a model computed with the revised Band Model opacity, while the dotted line represents a model used in our previous analyses. The model parameters are $T_{\rm eff}$ = 3200 K, log g = 0.0, C/O = 1.1, [O/H] = [N/H] = 0.0, ^{12}C/^{13}C = 25, and $V_{\rm mic}$ = 3.0 km s^{-1}

by four parameters, i.e. effective temperature, surface gravity, micro-turbulent velocity, and chemical composition.

The effective temperatures determined by OT96 using the Infrared Flux method are $T_{\rm eff}$ = 3080 K (TX Psc), 2790 K (V Aql), and 3180 K (BL Ori). However, the effective temperature scale of carbon stars is still controversial. The effective temperatures determined with different methods like lunar occultations, interferometry, the Infrared Flux method, and empirical color-$T_{\rm eff}$ relations do not necessarily show good agreement. In fact, the effective temperatures adopted by LGEH86 for these stars are 3030 K (TX Psc), 2610 K (V Aql), and 2960 K (BL Ori). But it seems unlikely that BL Ori has almost the same effective temperature with TX Psc, given their infrared colors. The $(J-L')_0$ colors are 1.65 for TX Psc and 1.42 for BL Ori (OT96). In view of the controversial temperature scale of carbon stars and the differences of the effective temperatures adopted in the analyses, we compute a grid of model atmospheres with two different effective temperature scales, and examine the effect on the resulting abundances. In one case, we adopt effective temperatures of 3100 K (TX Psc), 2800 K (V Aql), and 3200 K (BL Ori), while in the other case 3000 K (TX Psc), 2600 K (V Aql), and 3000 K (BL Ori), which are approximately the temperatures adopted by LGEH86.

The surface gravity of an individual carbon star is estimated from the stellar mass and the radius as follows.

$$\log g = \log g_{\odot} - 2\log(R/R_{\odot}) + \log(M/M_{\odot}) \quad (2)$$

In the case of TX Psc, the stellar radius can be relatively accurately derived, thanks to angular diameter measurements and the distance determined using the Hipparcos parallax. The results of angular diameter measurements show fair agreement with one another: 8.38 mas (Richichi et al. 1995), 11.2 mas (Dyck et al. 1996), 11.2 mas (Quirrenbach et al. 1994), 8.90 mas (de Vegt 1974), 9.00 mas (Lasker et al. 1973), and 10.2 mas (Dunham et al. 1975). Combining these values with the distance 230 pc (Hipparcos catalogue) results in $R = 200R_{\odot}$ – $270R_{\odot}$. The masses of Galactic carbon stars are estimated to be $1M_{\odot} < M <$ 2-3$M_{\odot}$ from the kinematical analyses by Dean (1976) and Wallerstein & Knapp (1998). This range also agrees with an estimate based on the scale height of the Galactic distribution of carbon stars by Claussen et al. (1987), $1.2M_{\odot} < M < 1.6M_{\odot}$. Assuming $M = 1M_{\odot}$ and $R = 270R_{\odot}$, we obtain the lower limit of $\log g = -0.4$. The combination of $M = 2M_{\odot}$ and $R = 200R_{\odot}$ corresponds to the upper limit of $\log g = +0.14$. In the light of these estimates, we adopt $\log g$ = 0.0 for TX Psc, and assume the same value for the other two stars as well. We also compute a grid of models with $\log g = -0.5$ for TX Psc, to check the effect of the uncertainty of surface gravity on the resulting abundances.

Table 2. Model grid assigned to each star

TX Psc				
$T_{\rm eff}$ (K)	3100	3000		
$\log g$ (cm s^{-2})	0.0	-0.5		
[O/H]	0.0	-0.3		
C/O	1.02	1.05	1.1	1.2
[N/H]	0.0	-0.3		
V Aql				
$T_{\rm eff}$ (K)	2800	2600		
$\log g$ (cm s^{-2})	0.0			
[O/H]	0.0	-0.3		
C/O	1.1	1.5	2.0	
[N/H]	-0.6	-0.9		
BL Ori				
$T_{\rm eff}$ (K)	3200	3000		
$\log g$ (cm s^{-2})	0.0			
[O/H]	0.0	-0.3		
C/O	1.05	1.1	1.2	1.5
[N/H]	0.0	-0.3		

As the next section will describe, the analysis of elemental C, N, and O abundances is done in a self-consistent way, taking account of the dependence of the atmospheric structure on the chemical composition, which is actually also an input parameter of models. With $T_{\rm eff}$ and $\log g$ assigned to each star, a grid of model atmospheres is computed with different combinations of $\log \varepsilon({\rm O})$, C/O, and $\log \varepsilon({\rm N})$. The grid of ([O/H], C/O, [N/H]) used for each star is shown in Table 2. The abundances of elements other than C, N, and O are assumed to be solar (Anders & Grevesse 1989).

Since we include the isotopic species bearing ^{13}C as opacity sources, a $^{12}{\rm C}/^{13}{\rm C}$ ratio should also be specified for the calculation of a model grid. We adopt $^{12}{\rm C}/^{13}{\rm C}$ = 25 for TX Psc and BL Ori, and 70 for V Aql. These values are based on the result derived by OT96, but they are set slightly higher than the values in OT96, in the light of the effect of the new models on the analysis of $^{12}{\rm C}/^{13}{\rm C}$ ratios. We will return to this point in Sect.7.

We adopt a micro-turbulent velocity of 3 km s^{-1} and the effect of turbulent pressure is included in the model computation. As the next section will show, the values derived from the self-consistent analysis range from 2.5 to 3.0 km s^{-1}, assuring this assumption.

5. CNO analysis

The standard procedure of an abundance analysis is to determine the correction for molecular abundances with respect to assumed values for each selected line by comparing predicted equivalent widths and observed ones. The equivalent widths are calculated by integrating synthetic spectra computed for each line using a model with pre-given abundances. The micro-turbulent velocity is determined so that the molecular abundance corrections for weak lines and moderately strong lines should be consistent. With an isotropic and depth-independent Gaussian micro-turbulent velocity assumed, we calculate the equivalent widths of selected lines with three micro-turbulent velocities[1], $\xi_{\rm mic}$ = 2, 3, and 4 km s^{-1}. Then the micro-turbulent velocity can be determined by interpolation from the three values above so that the molecular abundance corrections for all the lines should be independent of the line strengths. To determine the correction for the molecular abundance accurately, it is crucial to use both weak lines and medium strong lines. Fig. 9 illustrates an example of this procedure for ^{12}CO lines in TX Psc. The logarithmic molecular abundance corrections for the selected lines, designated δ(CO), are fitted with a quadratic function $\delta({\rm CO}) = A(\xi_{\rm mic}) + B(\xi_{\rm mic})X^2$, where X is defined as $X = \log(W/\omega)_{\rm obs} + 6.0$. W is the observed equivalent width and ω is the wavenumber of a line. Once the micro-turbulent velocity is determined so that B should be zero, A gives the molecular abundance correction to the assumed value.

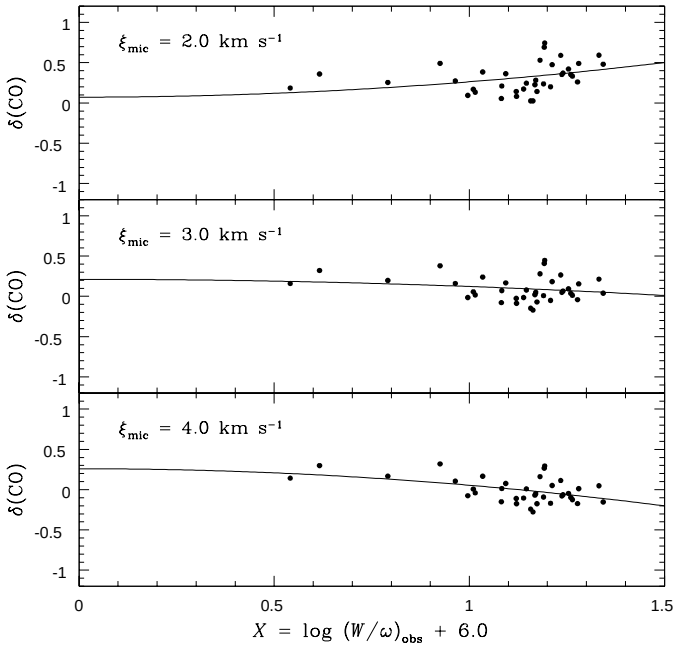

Fig. 9. An example of the standard analysis for CO lines in TX Psc. The logarithm of the correction for the molecular abundance $\delta({\rm CO})$ for each line is plotted against $X = \log(W/\omega)_{\rm obs} + 6.0$. A model with $T_{\rm eff}$ = 3100 K, $\log g$ = 0.0, [O/H]=0.0, C/O=1.1, [N/H]=0.0, $^{12}{\rm C}/^{13}{\rm C}$ = 25, and $V_{\rm mic}$ = 3.0 km s^{-1} is used

This procedure is also applied to CN lines, as shown in Fig. 10. The micro-turbulent velocities derived from CO and CN lines agree rather well. However, the scarcity of C_2 lines selected for the analysis makes it almost impossible to determine the micro-turbulent velocity independently. The application of the procedure described above would only lead to an erroneous or unreliable micro-turbulent velocity and an inaccurate correction for the C_2 abundance. Therefore, using the micro-turbulent velocity derived from CO and CN lines, we determine the abundance correction for C_2 by taking the mean of the corrections

[1] A micro-turbulent velocity adopted in model calculations is designated $V_{\rm mic}$, while one used in the calculations of line intensities $\xi_{\rm mic}$.

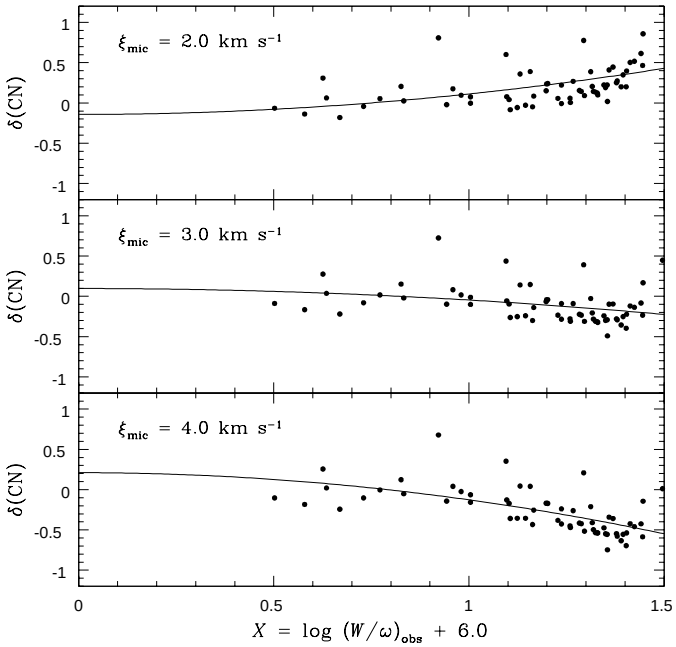

Fig. 10. An example of the standard analysis for CN lines in TX Psc. The logarithm of the correction for the molecular abundance $\delta(\mathrm{CN})$ for each line is plotted against $X = \log(W/\omega)_{\rm obs} + 6.0$. The model parameters are the same with those listed in the legend to Fig. 9

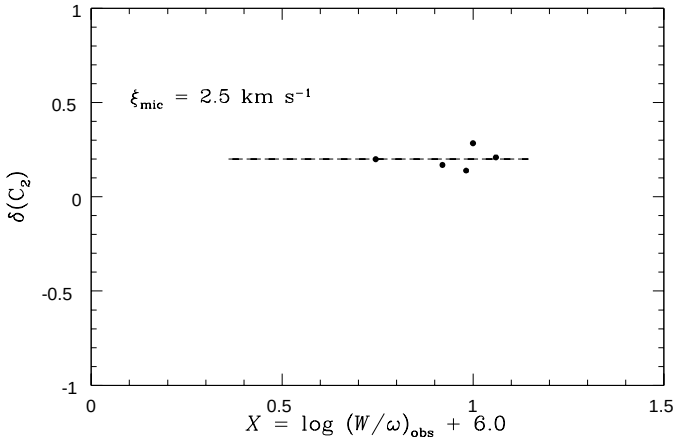

Fig. 11. An example of the analysis for C_2 lines in TX Psc. The logarithm of the correction for the molecular abundance $\delta(\mathrm{C_2})$ for each line is plotted against $X = \log(W/\omega)_{\rm obs}+6.0$. The model parameters are the same with those listed in the legend to Fig. 9, and $\xi_{\rm mic}$ = 2.5 km s^{-1} is assumed in calculating the equivalent widths. The dashed line shows the mean of the $\delta(\mathrm{C_2})$'s for the five lines

for the lines, instead of fitting with the above quadratic function. Fig. 11 illustrates this procedure for C_2 lines in TX Psc.

The atmospheric structure of carbon stars is sensitive to the chemical composition, especially C/O ratio. Fig. 12 shows the effect of C, N, and O abundances on temperature stratifications in the case of 3100 K models. It should be noted that the atmospheric structure is quite dependent on the oxygen abundance and, more importantly, C/O ratio. On the other hand, with most of nitrogen atoms locked up into spectroscopically inert N_2 molecules, the change of nitrogen abundance does not have a noticeable effect on the atmospheric structure. In order to determine C, N, and O abundances self-consistently, taking account of the effects of chemical composition on the atmospheric structure properly, we calculate a grid of model atmospheres with different combinations of [O/H], C/O, and [N/H] given in Table 2. The corrections for the molecular abundances, δ(CO), δ(CN), and $\delta(\mathrm{C_2})$ are evaluated with each model, together with the micro-turbulent velocity, using the procedure shown in Figs. 9, 10, and 11. The combination of [O/H], C/O, and [N/H] with which all of δ(CO), $\delta(\mathrm{C_2})$, and δ(CN) should be zero is determined by interpolation.

We first evaluate the molecular abundance corrections for CO, C_2, and CN, using models with different sets of ([O/H], C/O), but with a fixed nitrogen abundance, $[\mathrm{N/H}]_1$. The molecular abundance corrections, δ(CO), $\delta(\mathrm{C_2})$, and δ(CN), can be regarded as functions of [O/H] and C/O. As an example, $\delta(\mathrm{C_2})$ evaluated with each model is plotted as a function of [O/H] and C/O in Fig. 13. The intersection with the plane $\delta(\mathrm{C_2}) = 0$ (shown by the thick solid line in Fig. 13) represents the set of ([O/H], C/O) with which the correction for C_2 abundance should be zero. This intersection is represented by the filled circles in Fig. 14, which is actually the top view of Fig. 13. Likewise the open circles represent the curves on which δ(CO) should be zero. The intersection of the two curves, designated ($[\mathrm{O/H}]_1$, $(\mathrm{C/O})_1$), gives the oxygen and carbon abundances with which δ(CO) and $\delta(\mathrm{C_2})$ are simultaneously zero. Since δ(CN) has already been evaluated at each grid point and can be regarded as a function of [O/H] and C/O, the value of δ(CN) at ($[\mathrm{O/H}]_1$, $(\mathrm{C/O})_1$) is easily evaluated by interpolation. We refer to it as $\delta(\mathrm{CN})_1$. This procedure is repeated with another value of nitrogen abundance, $[\mathrm{N/H}]_2$, and we obtain $[\mathrm{O/H}]_2$ and $(\mathrm{C/O})_2$ together with $\delta(\mathrm{CN})_2$. The point where δ(CO), $\delta(\mathrm{C_2})$, and δ(CN) are simultaneously zero should be somewhere on the line between ($[\mathrm{O/H}]_1$, $(\mathrm{C/O})_1$, $[\mathrm{N/H}]_1$) and ($[\mathrm{O/H}]_2$, $(\mathrm{C/O})_2$, $[\mathrm{N/H}]_2$) in the 3-dimensional space of ([O/H], C/O, [N/H]). It can be derived by linear interpolation, and we designate it ([O/H], C/O, $[\mathrm{N/H}])_f$.

Exactly speaking, there is still another step concerning the self-consistent determination of the micro-turbulent velocity. As mentioned above, a fixed value of micro-turbulent velocity is used in the evaluation of $\delta(\mathrm{C_2})$. It should be noted here, however, that micro-turbulent velocity is determined simultaneously with the molecular abundance correction for each model. Namely, micro-turbulent velocity is also a function of [O/H], C/O, and [N/H]. Now that we have obtained ([O/H], C/O, $[\mathrm{N/H}])_f$, it is straightforward to evaluate the micro-turbulent velocity at this point by interpolation. The derived value should be consistent with that used for the evaluation of $\delta(\mathrm{C_2})$. If the micro-turbulent velocity interpolated at ([O/H], C/O, $[\mathrm{N/H}])_f$ differs significantly from that adopted in the evaluation of $\delta(\mathrm{C_2})$, the whole procedure should be repeated until the self-consistency of the determination of the micro-turbulent velocity is obtained.

The uncertainties which might arise from the interpolation procedure can be checked by computing the final model atmosphere with the C, N, and O abundances determined for each

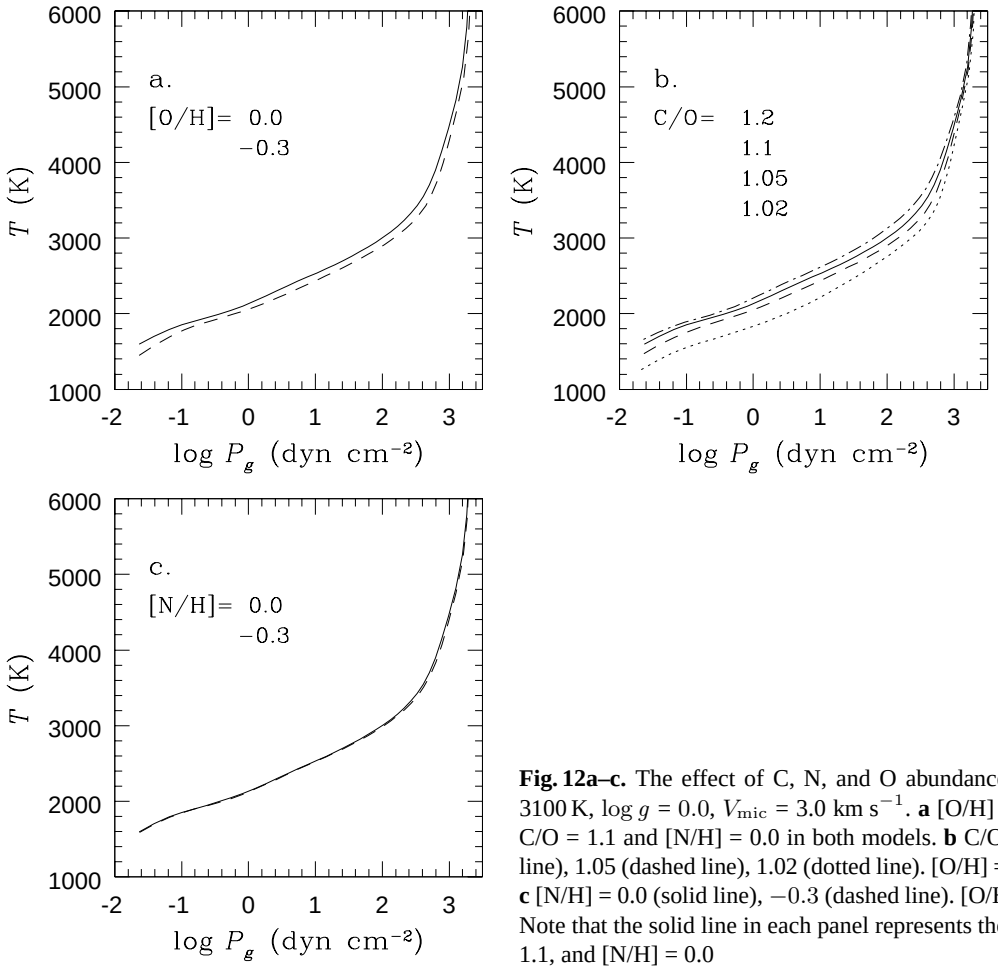

Fig. 12a–c. The effect of C, N, and O abundances on model atmospheres with $T_{\rm eff}$ = 3100 K, $\log g$ = 0.0, $V_{\rm mic}$ = 3.0 km s^{-1}. **a** [O/H] = 0.0 (solid line), -0.3 (dashed line). C/O = 1.1 and [N/H] = 0.0 in both models. **b** C/O = 1.2 (dotted-dashed line), 1.1 (solid line), 1.05 (dashed line), 1.02 (dotted line). [O/H] = 0.0 and [N/H] = 0.0 in all the models. **c** [N/H] = 0.0 (solid line), -0.3 (dashed line). [O/H] = 0.0 and C/O = 1.1 in both models. Note that the solid line in each panel represents the same model with [O/H] = 0.0, C/O = 1.1, and [N/H] = 0.0

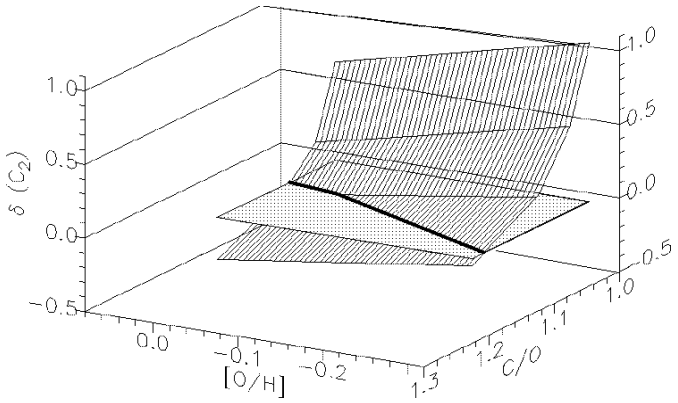

Fig. 13. $\delta(C_2)$'s evaluated with models with different sets of ([O/H], C/O) are plotted. The thick solid line shows the intersection where $\delta(C_2) = 0$

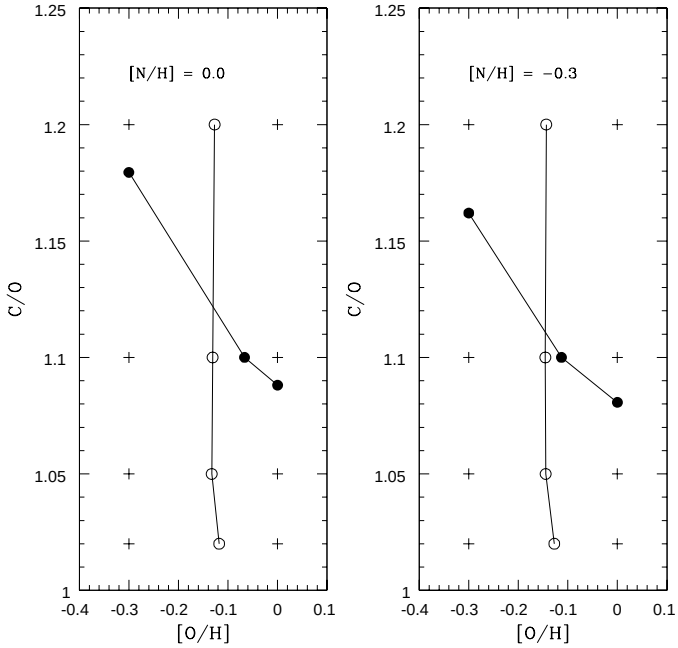

Fig. 14. Self-consistent analysis applied to TX Psc. The lines connecting the open circles represent the curves on which δ(CO) should be zero, while those connecting the filled circles represent the curves on which $\delta(C_2)$ should be zero. The cross hairs represent the model grid

star. We have computed the final model adjusted to each star, and confirmed that the lines of CO, C_2, and CN are simultaneously reproduced with these final models. This has turned out to assure that the interpolation procedure described above gives a consistent result.

The uncertainties of the resulting abundances arise from internal and external errors. Internal errors can be regarded as the

Table 3. The resulting C, N, and O abundances, and micro-turbulent velocities in three carbon stars. O: present work, L: Lambert et al. (1986)

Star	$T_{\rm eff}$ (K)	[O/H]		[C/H]		C/O		[N/H]		$\xi_{\rm mic}$ (km s^{-1})	
		O	L	O	L	O	L	O	L	O	L
TX Psc	3000	−0.15	−0.10	0.14	0.16	1.07	1.027	−0.19	−0.27	2.5	2.2
	3100	−0.14		0.16		1.17		−0.13		2.6	
V Aql	2600	−0.23	−0.20	0.19	0.15	1.47	1.25	−0.99	−0.65	2.9	2.0
	2800	−0.36		0.13		1.74		−0.72		2.9	
BL Ori	3000	−0.34	−0.29	−0.06	−0.02	1.07	1.039	0.00	0.05	2.6	2.0
	3200	−0.28		0.05		1.19		0.08		2.7	

errors resulting from the scatter of the lines in the simultaneous determination of the molecular abundance correction and the micro-turbulent velocity shown in Figs. 9, 10, and 11. The internal errors of the oxygen abundances in TX Psc, V Aql, and BL Ori are about 0.06 dex, 0.16 dex, and 0.15 dex, respectively. The internal errors of the nitrogen abundances are also dominated by the scatter of the lines. We estimate them to be about 0.1 dex, 0.17 dex, and 0.1 dex for TX Psc, V Aql, and BL Ori, respectively. The errors of C/O ratios are somewhat difficult to estimate, because the number of the selected C_2 lines is limited. The nominal internal errors resulting from the scatter of the lines in the analysis such as shown in Fig. 11 are 0.1%, 10%, and 10% for TX Psc, V Aql, and BL Ori, respectively.

External errors arise from the uncertainties of the stellar parameters adopted in the analysis and the atmospheric structure itself, in other words, the validity of model atmospheres. In the next section, we will discuss the effects of effective temperature and surface gravity on the resulting abundances.

6. Result

Table 3 summarizes the resulting C, N, and O abundances in three stars. The result derived by LGEH86 is also given for comparison. If the same effective temperatures are adopted, the resulting abundances derived by the both groups agree rather well. The oxygen abundances are in agreement within the bounds of uncertainty of the results. Despite the apparent good agreement of the carbon abundances themselves, the C/O ratios derived here are somewhat larger than those obtained by LGEH86. The differences seem to be insignificant, but even a slight change in C/O ratio has a large effect on the atmospheric structure, especially if the C/O ratio is close to 1. Therefore, these differences should not necessarily be regarded to be negligible. As to the nitrogen abundances, the differences are about 0.1 dex for TX Psc and BL Ori, but more than 0.3 dex for V Aql. In the calculation of the equivalent widths of CN lines, we use the same oscillator strengths and dissociation energy with those adopted by LGEH86. Therefore the difference cannot be attributed to the differences of the relevant molecular data. The molecular abundance of CN is determined not only by the nitrogen abundance but also by the amount of carbon not locked up into CO molecules. The difference of C/O ratio in V Aql between LGEH86 and the present work is rather large as compared with TX Psc and BL Ori. The higher C/O ratio leads to the higher abundance of CN in the atmosphere. This might be responsible for the lower nitrogen abundance in this star.

Table 4. C, N, and O abundances in TX Psc derived using models with $T_{\rm eff}$ = 3000 K and $\log g = -0.5$

Star	[O/H]	[C/H]	C/O	[N/H]
TX Psc	−0.31	−0.01	1.10	−0.29

If the higher effective temperature scale is adopted, the C/O ratios are higher than those derived by LGEH86. Our C/O ratios are about 1.1 or larger, in contrast to LGEH86's conclusion that the majority of carbon stars have C/O ratios rather close to 1. However, the C/O ratios derived here are not as high as the values derived by OTAY98. The high C/O ratios reported by OTAY98 in these three stars are mostly due to the warmer model atmospheres induced by the underestimate of the mean line separations as discussed in Sect. 4. As Figs. 7 and 8 show, the revision of the Band Model opacity results in the cooler atmospheres, where the abundance of C_2 is higher compared with our previous models. It leads to the smaller C/O ratios as compared with the result derived by OTAY98.

We examine the effect of the uncertainties of stellar parameters below. Since we have constructed two grids of models with different effective temperatures for each star, it is straightforward to estimate the effect of the uncertainty of effective temperature. Namely, it is represented by the results derived with different effective temperatures given in Table 3. The uncertainty of $T_{\rm eff}$ by 200 K leads to a difference of at most 0.13 dex in the oxygen abundances. The C/O ratios are affected by 10 to 15% for the same amount of the uncertainty of $T_{\rm eff}$. The effects on the resulting nitrogen abundances are less than 0.1 dex for TX Psc and BL Ori, and 0.26 dex for V Aql.

Next we examine the effect of the uncertainty of surface gravity. For TX Psc, we calculate a grid of model atmospheres with $T_{\rm eff}$ = 3000 K and $\log g = -0.5$. A surface gravity of $\log g = -0.5$ can be considered to be the lower limit, maybe not realistic given the estimates of its stellar radius and stellar mass. Therefore, the abundances derived with models with $\log g = -0.5$ should be regarded to represent the maximum effect of the uncertainty of surface gravity. The resulting C, N, and O abundances are given in Table 4. The decrease of surface gravity leads to the decreases of the resulting C, N, and O abundances by about 0.1 to 0.15 dex. However, the C/O ratio increases from 1.07 to 1.10. Though the difference between C/O = 1.07 and 1.1

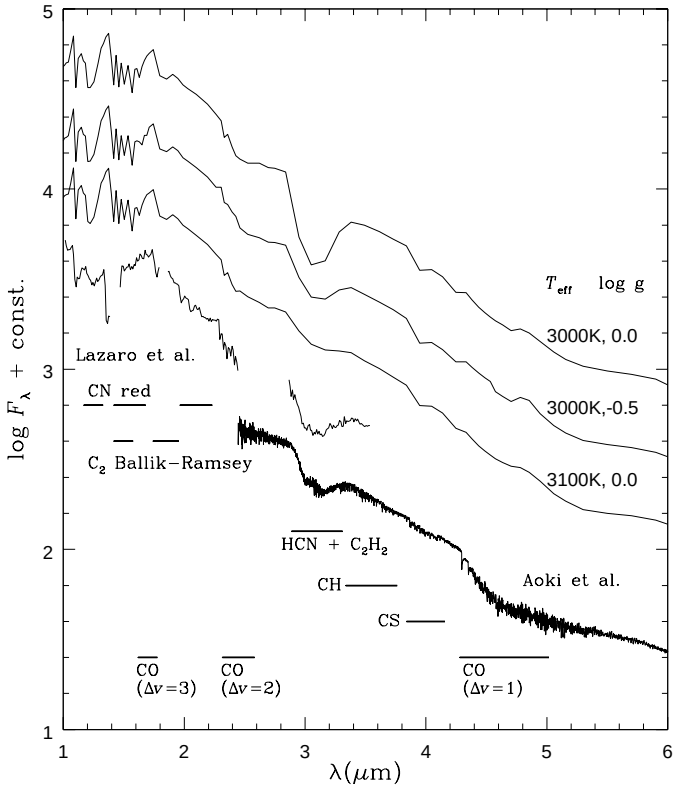

Fig. 15. Comparison between the emergent fluxes predicted from the models adjusted to TX Psc and spectrophotometric observations. Note that three models have different C, N, and O abundances. The fluxes are shifted in the vertical coordinate for clarity of presentation. See also the text

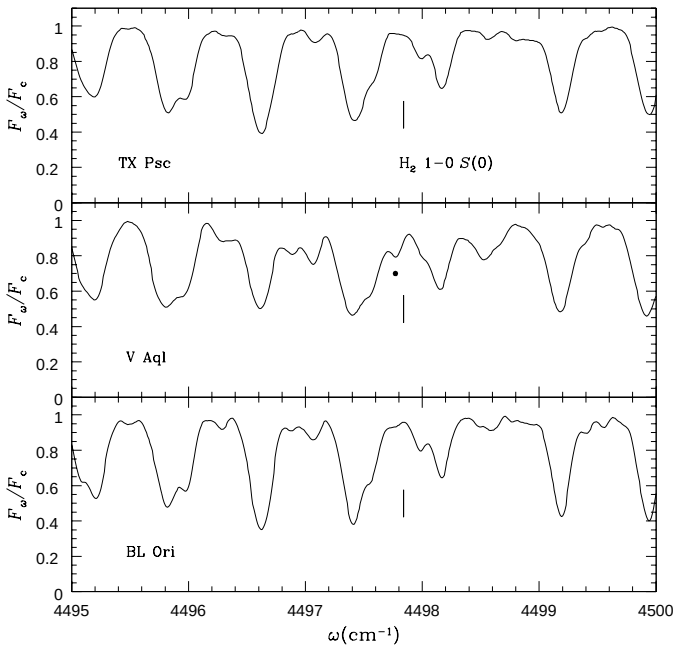

Fig. 16. A portion of spectra of TX Psc, V Aql, and BL Ori in the region where the H_2 1-0 $S(0)$ line is located. The spectra are already shifted to the laboratory system. The position of the H_2 line is indicated by the ticks, while the observed position of the line in V Aql is indicated by the filled circle

might seem to be insignificant, it actually has a large effect on the atmospheric structure. Since CO is the most stable molecule in the relevant temperature and pressure ranges, the amounts of molecules except for CO are governed by $(\mathrm{C/O}-1)\times\varepsilon(\mathrm{O})$. Therefore, (C/O − 1) is a better indicator of the effects on the atmospheric structure. In fact, the emergent fluxes predicted by these models exhibit the effect of C/O ratio clearly. This will be discussed in comparison with spectrophotometric observations in the next section.

7. Discussion

7.1. Tests of model atmospheres

In this subsection, we examine the validity of the model atmospheres, using observed spectral energy distributions as well as some spectral lines.

Fig. 15 shows a comparison of the emergent fluxes predicted by the models adjusted to TX Psc with spectrophotometric observations: an observation with the Infrared Space Observatory (ISO) by Aoki et al. (1998) and a ground-based observation by Lázaro et al. (1994). Major molecular absorption features are also indicated. As the previous section shows, the resulting C, N, and O abundances are rather sensitive to the stellar parameters – $T_{\rm eff}$ and $\log g$ – adopted in the analysis. We have derived the C, N, and O abundances with three different sets of $T_{\rm eff}$ and $\log g$: (3000, 0.0), (3100, 0.0), and (3000, -0.5). The emergent fluxes predicted by these three models are shown in Fig. 15. It should be kept in mind that these three models have different C, N, and O abundances, corresponding to the results given in Tables 3 and 4. The figure illustrates that the absorption features due to diatomic molecules are rather insensitive to $T_{\rm eff}$ and $\log g$, and the observed strengths are fairly reproduced by the models. On the other hand, the 3 μm feature due to HCN and C_2H_2 is very sensitive to $T_{\rm eff}$ and $\log g$. It should be noted that changes in $T_{\rm eff}$ and $\log g$ affect the strength of the 3 μm feature also through their effects on the resulting C, N, and O abundances. The changes of C, N, and O abundances lead to the change of the atmospheric structure, which affects the predicted strength of the 3 μm feature. As the figure shows, however, it is difficult to disentangle the effects of $T_{\rm eff}$ and $\log g$ on the 3 μm feature, and to derive a unique set of ($T_{\rm eff}$, $\log g$). The effective temperature should be between 3000 and 3100 K, while the surface gravity should be between -0.5 and 0.0. These ranges are well within the bounds of accuracy of the estimated effective temperature and surface gravity, therefore, the analysis is consistent in this sense.

The H_2 1-0 $S(0)$ line at 2.2 μm is supposed to provide us with an opportunity to check model atmospheres. Fig. 16 shows a portion of spectra where the H_2 line is observed. A glance of the figure reveals that the H_2 lines in TX Psc and BL Ori are not to be clearly recognized. On the other hand, V Aql exhibits the H_2 line relatively clearly. We computed the strength of the H_2 line using the model adjusted to V Aql, but the line predicted by the model is much weaker than the observed. However, it might

not necessarily undermine the validity of photospheric models. Namely, Ohnaka (1997) reveals that the H_2 line in V Aql shows a redshift of 2–3 km s^{-1} as compared with those of weak lines of the CO second-overtone bands, which are formed in deep layers in the photosphere. It suggests that the H_2 line might be formed not only in the photosphere but also in the so-called warm molecular envelope whose existence was recognized in the absorption excess of low excitation lines of the CO first-overtone bands by Tsuji (1988) in the case of M giants and by recent observations with the ISO (e.g. Tsuji et al. 1997 for M giants and Aoki et al. 1998 for carbon stars). In the light of the picture of the outer atmosphere drastically revised by these observations, the H_2 line is not necessarily adequate for examining model atmospheres.

CH lines around 4 μm also provide us with an opportunity to test the consistency of the model atmospheres and the analysis. LGEH86 show that the CH lines predicted by their models are stronger than the observed: the predicted strengths of CH 1-0 lines are $\log(W/\omega) \sim -4.8$, while the observed ones are about $\log(W/\omega) \sim -5.1$. We calculated the strengths of CH 1-0 lines using the model adjusted to each star analyzed here. It has turned out that the predicted CH lines are still stronger than the observed, in spite of the differences of the effective temperature and C/O ratio between LGEH86 and the present work. In fact, the predicted strengths of the CH lines are almost the same with those presented in LGEH86. The oscillator strengths are based on the same reference (Lie et al. 1973). Mild hydrogen deficiency might solve the discrepancy, but it should be examined, after final models for the program stars are computed using the abundances determined with a grid of hydrogen poor models. According to LGEH86, a decrease of hydrogen by 3 dex is needed to reproduce the observed strengths of the CH lines. On the other hand, as Sect. 3 shows, the oscillator strengths of C_2 molecule is still in dispute. If the larger oscillator strengths based on the ab initio calculation were adopted, the carbon abundances would be lower than the values derived in the present work. With a lower carbon abundance, the CH lines might be weaker than discussed above, which might reconcile the disagreement with the observation. The discrepancy in CH lines should be worth further investigation.

As we have discussed in this subsection, it is difficult to fit the observed spectral features perfectly with the current models. Some of these problems can be reconciled by adjusting the stellar parameters like $T_{\rm eff}$ and $\log g$ within the limits of accuracy of their determination. However, as the case of the H_2 line demonstrates, it is necessary to construct a comprehensive model from the photosphere to the outer atmosphere, in order to interpret the unexplained behavior of some spectral lines.

7.2. Accuracy of elemental C, N, and O abundances and C/O ratio

The accuracy of stellar abundance analyses cannot be very high in general. It may be about within ± 0.2 – 0.3 dex in main sequence stars except for very hot as well as very cool stars, and such accuracy as ± 0.1 dex can be achieved only in limited cases (e.g. Baschek 1991). In fact, abundance analyses have been done on the same object by several different groups, but the resulting abundances show a large difference in general (e.g. Cayrel de Strobel et al. 1997). In the case of cool stars, typical systematic errors in a chemical analysis may be about 0.3 dex or greater from intercomparisons among different studies (e.g. Gustafsson 1989).

The abundance analyses of cool evolved stars such as carbon stars have been deemed the most difficult, and few quantitative analyses have been done so far. For cool carbon stars, LGEH86 is almost the only work to be compared with our analysis. Although we used the same observational data and, purposely, the same molecular data with LGEH86, the method of our analysis as well as model atmospheres used are quite independent of those used by LGEH86. Especially, we have examined the interplay between abundance determination and model atmospheres in detail. This should be an important step especially for quantitative analyses of the molecular spectra of cool carbon stars, in view of the strong dependence of a model atmosphere on abundances and vice versa. It is remarkable, therefore, that we agree rather well with LGEH86 within ± 0.1 dex in most cases, if the same stellar parameters and molecular data are adopted. As a result, our self-consistent analysis lends a support to LGEH86's result, and demonstrates that elemental abundances in cool carbon stars can be determined with accuracy at least comparable with those in other types of stars.

It should be kept in mind, however, that the resulting abundances are rather sensitive to the external error sources. It should also be stressed that our C/O ratios are somewhat higher than LGEH86's results, even if the same stellar parameters and molecular data are adopted. Moreover, the effective temperature scale may be higher by 100–200 K than adopted by LGEH86. In that case, C/O ratios in three stars are about 1.1 or larger, in contrast with the result derived by LGEH86 that the majority of carbon stars have C/O ratios rather close to 1. In view of the chemistry of the photosphere and the circumstellar envelope, even a slight difference of C/O ratio has a drastic effect, especially if the C/O ratio is near 1. At the same time, the internal errors of C/O ratios are already about 10%, which can be translated to a difference between C/O = 1.02 and 1.1. Namely, though very accurate determination of C/O ratio is required for the research of chemical and physical processes in the circumstellar envelope like grain formation and mass outflow, it is still a formidable task to achieve such accuracy. Besides, the molecular data of C_2 and CN are still controversial, which would also bring about systematic uncertainties. In order to suppress external errors in abundance analyses, it would be indispensable to determine stellar parameters accurately. It would require, for example, a simultaneous observation of angular diameters and bolometric fluxes for the accurate determination of effective temperatures.

7.3. Effects of the new opacity on $^{12}C/^{13}C$ ratios

As Sect. 4.1 reveals, the revision of molecular opacity leads to cooler atmospheres than those used in our previous analyses.

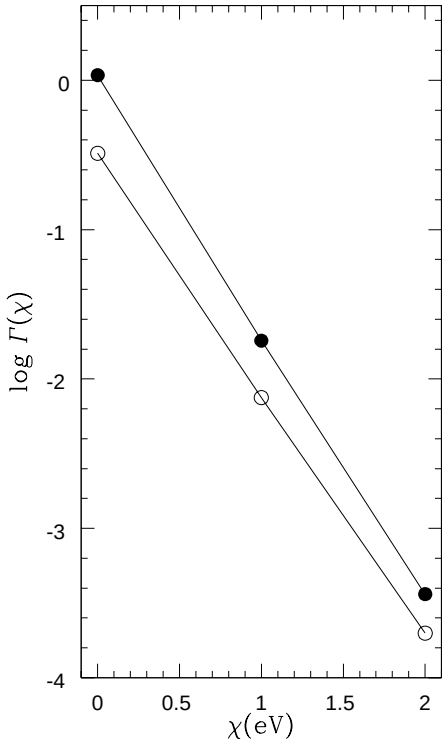

Fig. 17. $\Gamma(\chi)$ calculated with models used in OT96 (open circles) and in the present work (filled circles)

We also examine its effect on the $^{12}C/^{13}C$ ratios derived by OT96. As Figs. 11, 12, and 13 in OT96 show, $^{12}C/^{13}C$ ratios can be derived by measuring the horizontal shift between the curves of depth growth for ^{12}CN and ^{13}CN lines. The abscissa is $\log(gf\Gamma)$, where g and f is the statistical weight and the oscillator strength of a line, respectively. $\Gamma(\chi)$ is a line intensity predicted with the weighting function method (e.g. Cayrel & Jugaku 1963) for a fictitious line with a gf-value of 1 and a lower excitation potential (LEP) of χ. The effect of the difference of atmospheric structures would appear in Γ.

Fig. 17 shows predicted line intensities $\Gamma(\chi)$ calculated with a model used in OT96 and one used in the present work. Both models have the same set of parameters: $T_{\rm eff}$ = 3000 K, $\log g$ = 0.0, C/O = 1.1, [O/H] = 0.0, [N/H] = 0.0, and $V_{\rm mic}$ = 3.0 km s^{-1}. The ^{12}CN lines used in the determination of $^{12}C/^{13}C$ ratios in N-type carbon stars by OT96 have LEP's of about 1.2 eV, while the ^{13}CN lines have LEP's of about 0.0 eV. Therefore, $\Gamma(0.0\,\mathrm{eV}) - \Gamma(1.2\,\mathrm{eV})$ represents the effect of the difference of model atmospheres on the resulting $^{12}C/^{13}C$ ratios. It should be noted that the absolute value of Γ does not matter, because $^{12}C/^{13}C$ ratios are determined from the horizontal *shift* between the curves of depth growth for ^{12}CN and ^{13}CN lines. In the case shown in Fig. 17, $\Gamma(0.0\,\mathrm{eV}) - \Gamma(1.2\,\mathrm{eV})$ calculated with the new model has turned out to be larger by 40% than the one calculated with the model used in OT96. Thus it is expected that $^{12}C/^{13}C$ ratios become by about 40% larger than those derived by OT96. We calculate Γ using the final model atmosphere adjusted to each star, and re-determine $^{12}C/^{13}C$ ratios. Table 5 shows the $^{12}C/^{13}C$ ratios corrected with the new model atmospheres for TX Psc, V Aql, and BL Ori, together with the values derived by LGEH86. The table shows that the disagreement of $^{12}C/^{13}C$ ratios has been lessened. For example, we derived $^{12}C/^{13}C$ = 22 for TX Psc, while LGEH86 derived 43. If the new model atmosphere is used, the ratio is 31, closer to the value derived by LGEH86, but still lower than their value.

Table 5. Revised $^{12}C/^{13}C$ ratios in TX Psc, V Aql, and BL Ori

Star	OT96	this work	LGEH86
TX Psc	22	31	43
V Aql	66	74	82
BL Ori	26	35	57

As mentioned in Sect. 4.2, the $^{12}C/^{13}C$ ratios adopted in the model computation are not exactly the same as the values given in Table 5, but this slight difference would not lead to any noticeable change in the resulting C, N, and O abundances.

7.4. Determination of $^{12}C/^{13}C$ ratios from the FTS spectra

We also tried to determine $^{12}C/^{13}C$ ratios using ^{13}CO lines of the first- and second-overtone bands as well as ^{13}CN lines from the FTS spectra. Now that we have already determined the carbon abundance (^{12}C) in each star, it should be straightforward to derive $^{12}C/^{13}C$ ratios. Using the model atmosphere adjusted to each star, the molecular abundance correction for ^{13}CO or ^{13}CN is computed, and $\delta(^{13}\mathrm{CO})$ and $\delta(^{13}\mathrm{CN})$ should give $^{12}C/^{13}C$ ratios. However, it turned out that $\delta(^{13}\mathrm{CO})$'s and $\delta(^{13}\mathrm{CN})$'s computed for the selected lines do not give any consistent value. Namely, $\delta(^{13}\mathrm{CO})$'s and $\delta(^{13}\mathrm{CN})$'s vary from line to line as much as by an order of magnitude, therefore, no reliable $^{12}C/^{13}C$ can be derived, while the uncertainties of the $^{12}C/^{13}C$ ratios determined by LGEH86 are reportedly about 10 or 20%. This problem was already pointed out by Kipper et al. (1996), who analyzed the FTS spectrum of a carbon star, TU Gem, and found that the ^{13}CN lines they identified give widely different $^{12}C/^{13}C$ ratios. As they point out, the large spread might be due to unidentified blending, and a comparison of the lines selected for these analyses might also help clarify the reasons for the discrepancies.

7.5. Carbon star formation

We discuss the formation of carbon stars based on the results of our analyses of $^{12}C/^{13}C$ ratios and C/O ratios. In Fig. 18, C/O ratios are plotted against $^{12}C/^{13}C$ ratios for the stars studied here. We adopt the result derived with the higher effective temperature scale, which is close to that determined by OT96, for the 3 μm feature is not well reproduced by the final model with the abundances derived with the lower effective temperature as Fig. 15 shows. The dashed lines represent the changes of $^{12}C/^{13}C$ and C/O ratios predicted by addition of ^{12}C to the atmosphere of M giants. The sets of ($^{12}C/^{13}C$, C/O) shown in the figure are the values assumed in M giants, based on the analysis by Smith & Lambert (1990). In these predictions it is assumed

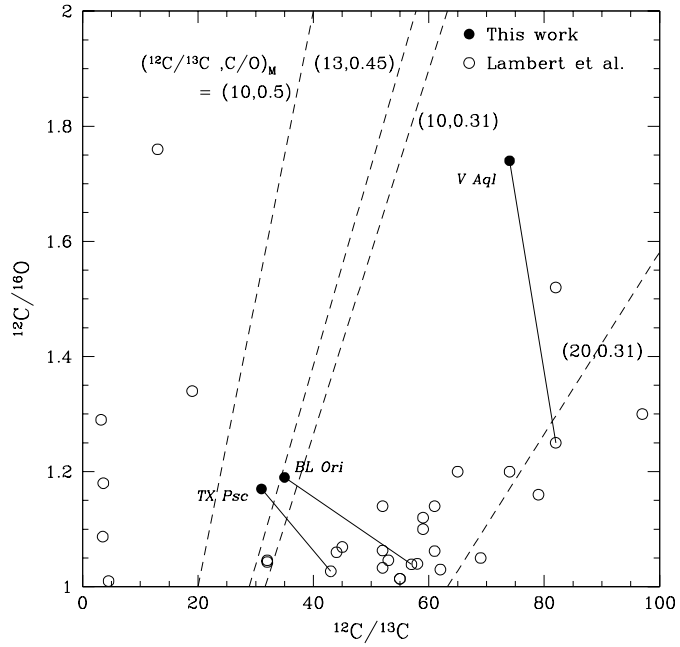

Fig. 18. C/O ratios plotted against $^{12}\mathrm{C}/^{13}\mathrm{C}$ ratios. The filled circles represent the results derived in the present work, while the open circles the results derived by LGEH86. The dashed lines are predictions estimated by pure ^{12}C addition to the atmosphere of M giants. The initial values of $^{12}\mathrm{C}/^{13}\mathrm{C}$ and C/O ratios assumed in M giants are also shown

that only ^{12}C is added to the stellar surface. The C/O ratios derived in the present work are higher than those derived by LGEH86, but the $^{12}\mathrm{C}/^{13}\mathrm{C}$ and C/O ratios in the three stars still fall within the limits of the predictions, supporting the scenario in which the thermal pulse and the third dredge-up are responsible for the formation of carbon stars. However, ^{16}O as well as ^{12}C is synthesized in the thermal pulse and dredged-up into the surface. In this case, the gradient of the change of C/O is smaller than in the case of pure ^{12}C addition (Herwig 1998), depending on stellar masses. It should be noted that there are still some uncertainties in the theoretical calculations of the evolution of AGB stars. Recent advance in evolutionary calculations like the inclusion of convective overshooting (e.g. Herwig 1998) suggests that stars with masses larger than $\sim 3M_{\odot}$ evolve to carbon stars. Straniero et al. (1997) show that stars with $M \geq 1.5M_{\odot}$ evolve to carbon stars unless extreme mass-loss rates are assumed. In view of these works, the difficulty in reproducing carbon stars with low masses has gradually been eased, while the estimates based on observations suggest somewhat smaller masses, as mentioned in Sect. 4.2.

The nitrogen abundances in TX Psc and V Aql are sub-solar, while it is almost solar in BL Ori. The nitrogen abundance increases by about 0.3 dex after the first dredge-up (e.g. Iben & Renzini 1983), therefore, it would be larger than the solar value, if the initial nitrogen abundances in these carbon stars were solar. However, given the result that the oxygen abundances are also sub-solar, these stars might have been formed in a rather metal-poor environment, which means that the initial nitrogen abundances might also have been sub-solar. The relation between [Fe/H] and [O/H] found in the Galaxy suggests that [O/H] ~ -0.2 should correspond to [Fe/H] $-0.3 \sim -0.5$ (e.g. Chiappini et al. 1999 and references therein). On the other hand, Chiappini et al. (1999) show that [N/Fe] is roughly zero and constant between [Fe/H] ~ -2 and 0. It translates to [N/H] ~ -0.5. Therefore, with a simplified assumption that the oxygen abundance is not much affected by the first and third dredge-ups, the increase of nitrogen brought about by the first dredge-up might explain the nitrogen abundances derived for the three stars. But it is still difficult to explain the low nitrogen abundance in V Aql, and in the case of BL Ori, small enhancement of nitrogen in addition to the first dredge-up might be implied.

At the same time, nitrogen abundance is supposed to be an indicator of the operation of the CN-cycle, which leads to an enhancement of nitrogen and a decrease of $^{12}\mathrm{C}/^{13}\mathrm{C}$ ratio. The nitrogen abundance in V Aql, which has a large $^{12}\mathrm{C}/^{13}\mathrm{C}$ ratio, is relatively low, while TX Psc and BL Ori show no significant depletion of nitrogen and have smaller $^{12}\mathrm{C}/^{13}\mathrm{C}$ ratios. As discussed above, however, the nitrogen abundances in three stars could be explained by the effect of the first dredge-up, and there is no clear implication of the operation of the CN-cycle at the AGB. It is premature to draw any conclusion from the results for only three stars. It is absolutely necessary to analyze more stars in order to clarify the tendency of nitrogen abundances in carbon stars. The definitive determination of the oscillator strengths and the dissociation energy of CN would also be indispensable.

8. Concluding remarks

We have determined elemental C, N, and O abundances in three carbon stars in a self-consistent way, with the interplay between the chemical composition and its effects on the atmospheric structure properly taken into account. If the effective temperatures are set to be the same with those adopted in LGEH86, the resulting carbon and oxygen abundances show good agreement with their results, typically within 0.1 dex. However, it should be noted that the C/O ratios derived here are still somewhat higher than their values. The nitrogen abundances are also in fair agreement with their results, except for V Aql, where the difference is more than 0.3 dex.

The changes of the stellar parameters like $T_{\rm eff}$ and $\log g$ have a rather large effect on the resulting C, N, and O abundances. The adoption of an effective temperature scale higher by 100–200 K, which is well possible for the stars studied here, leads to higher C/O ratios, 1.1 or larger. A decrease in surface gravity also leads to higher C/O ratios. The $^{12}\mathrm{C}/^{13}\mathrm{C}$ ratios have also been revised in the present work with the new model atmospheres. The $^{12}\mathrm{C}/^{13}\mathrm{C}$ ratios have turned out to be larger by about 40% than derived by OT96. We must, however, keep in mind that the spectra of cool carbon stars cannot be fully understood within the framework of the classical theory of line formation, some examples of which have been addressed in the text. Thus, further careful studies of the spectra and the atmospheric structure of cool carbon stars should still be followed.

The $^{12}\mathrm{C}/^{13}\mathrm{C}$ ratios and C/O ratios in three stars fall within the range predicted by the scenario where carbon stars are

formed by the dredge-up of ^{12}C synthesized in the thermal pulse. The sub-solar oxygen abundances found in three stars imply that these stars may have been formed in a somewhat metal-poor environment. The increase of nitrogen brought about by the first dredge-up could also explain the sub-solar or solar nitrogen abundances derived for these stars. At the same time, the nitrogen abundances do not clearly suggest the operation of the CN-cycle at the AGB.

Acknowledgements. We thank Dr. K. H. Hinkle for kindly providing us with the FTS spectra. K.O. is a Research Fellow of the Japan Society for the Promotion of Science (JSPS), and W.A. was also supported by the JSPS during this work.

References

Anders E., Grevesse N., 1989, Geochim. Cosmochim. Acta 53, 197
Aoki W., Tsuji T., Ohnaka K., 1998, A&A 340, 222
Baschek B., 1991, In: the Proceedings of IAU Symposium 145 "Evolution of Stars: The Photospheric Abundance Connection", eds. Michaud G., Tutukov A.V., Kluwer Academic Publishers, Dordrecht, p.39
Bauer W., Becker R.H., Hubrich C., Meuser R., Wildt J., 1985, ApJ 296, 758
Bauschlicher C.W.Jr., Langhoff S.R., Taylor P.R., 1988, ApJ 332, 531
Cayrel R., Jugaku J., 1963, Ann d'Astrophys 26, 495
Cayrel de Strobel G., Soubiran C., Friel E.D., Ralite N., François P., 1997, A&AS 124, 299
Cerny D., Bacis R., Guelachvili G., Roux F., 1978, J. Mol. Spectrosc. 73, 154
Chiappini C., Matteucci F., Beers T., Nomoto K., 1999, ApJ 515, 226
Claussen M.J., Kleinmann S.G., Joyce R.R., Jura M., 1987, ApJS 65, 385
Costes M., Naulin C., Dorthe G., 1990, A&A 232, 270
Davis S.P., Shortenhaus D., Stark G., Engleman R.Jr., Phillips J.G., Hubbard R.P., 1986, ApJ 303, 892
Davis S.P., Smith W.H., Brault J.W., Pecyner R., Wagner J., 1984, ApJ 287, 455
Dean C.A., 1976, AJ 81, 364
de Vegt Chr., 1974, A&A 34, 457
Douay M., Nietmann R., Bernath P.F., 1988, J. Mol. Spectrosc. 131, 250
Dunham D.W., Evans D.S., Silverberg E.C., Wiant J.R., 1975, MNRAS 173, 61P
Dyck H.M., van Belle G.T., Benson J.A., 1996, AJ 112, 294
Grevesse N., Lambert D.L., Sauval A.J., van Dischoeck E.F., Farmer C.B., Norton R.H., 1991, A&A 242, 488
Gustafsson B., 1989, ARA&A 27, 701
Herwig F., 1998, Ph.D. thesis, Christian-Albrechts-Universität zu Kiel
Hosinsky G., Klynning L., Lindgren B., 1982, Physica Scripta 25, 291
Iben I.Jr., Renzini A., 1983, ARA&A 21, 271
Kipper T., Jørgensen U.G., Klochkova V.G., Panchuk V.E., 1996, A&A 306, 489
Lambert D.L., Gustafsson B., Eriksson K., Hinkle K.H., 1986, ApJS 62, 373 (LGEH86)
Langhoff S.R., Bauschlicher C.W.Jr., Rendell A.P., Komornicki A., 1990, J.Chem.Phys. 92, 300
Larsson M., Siegbahn P.E.M., Ågren H., 1983, ApJ 272, 369
Lasker B.M., Bracker S.B., Kunkel W.E., 1973, PASP 85, 109
Lázaro C., Hammersley P.L., Clegg R.E.S., Lynas-Gray A.E., Mountain C.M., Zadrozny A., Selby M.J., 1994, MNRAS 269, 365
Lie G.C., Hinze J., Liu B., 1973, J. Chem. Phys. 59, 1887
Norton R.H., Beer R., 1976, J. Opt. Soc. America 66, 259
Ohnaka K., 1997, Ph.D. thesis, The University of Tokyo
Ohnaka K., Tsuji T., 1996, A&A 310, 933 (OT96)
Ohnaka K., Tsuji T., Aoki W., Yamamura I., 1998, Ap&SS 255, 369 (OTAY98)
Quirrenbach A., Mozurkewich D., Hummel C.A., Buscher D.F., Armstrong J.T., 1994, A&A 285, 541
Richichi A., Chandrasekhar T., Lisi F., Howell R.R., Meyer C., Rabbia Y., Ragland S., Ashok N.M., 1995, A&A 301, 439
Smith V.V., Lambert D.L., 1990, ApJS 72, 387
Sneden C., Lambert D.L., 1982, ApJ 259, 381
Straniero O., Chieffi A., Limongi M., Busso M., Gallino R., Arlandini C., 1997, ApJ 478, 332
Tsuji T., 1994, In: Molecular Opacities in the Stellar Environment, ed. Jørgensen U.G., Lecture Notes in Physics, Springer-Verlag, p.79
Tsuji T., 1986, A&A 156, 8
Tsuji T., 1988, A&A 197, 185
Tsuji T., 1991, A&A 245, 203
Tsuji T., Ohnaka K., Aoki W., Yamamura I., 1997, A&A 320, L1
Wallerstein G., Knapp G.R., 1998, ARA&A 36, 369